Parameter optimization of forward sound propagation models using Bayesian inference for sound field control purposes

Caviedes Nozal, Diego; Brunskog, Jonas

Published in:
Euronoise 2018 Proceedings

Publication date:
2018

Document Version
Peer reviewed version

Paramater optimization of forward sound propagation models using Bayesian inference for sound field control purposes

Diego Caviedes-Nozal
Acoustic Technology Group, Department of Electrical Engineer, Technical University of Denmark, Kongens Lyngby, Denmark.

Jonas Brunskog
Acoustic Technology Group, Department of Electrical Engineer, Technical University of Denmark, Kongens Lyngby, Denmark.

Abstract
Sound field control in outdoor concerts requires accurate estimates of the transfer functions between sources and receivers. Feed forward approaches are based on direct measurements of the transfer functions in a dense grid of points. This makes them intractable for large scale situations, showing the need of propagation models in order to characterize the sound field in such large areas. Uncertainty in the parameters introduced in the propagation models, such as meteorological, acoustical and geometrical ones, lead to inaccurate estimates of the transfer functions and therefore to a poor performance of the sound field control strategy. In this paper we present first results of the method introduced by Heuchel et al. [1] to increase the accuracy of the predictions. The parameters of the propagation model are optimized through auxiliary measurements and Bayesian inference.

PACS no. 43.60.Np, 43.60.Pt

1. Introduction

The performance of sound field control techniques strongly relies on the precision of the estimation of the transfer functions between sources and control areas [2]. The most reliable procedure to get the transfer functions is to directly measure them, where the control areas need to be densely sampled in order to avoid aliasing. This is not feasible for outdoor concerts because the areas to be controlled are large.

An alternative method to calculate the transfer functions is to use sound propagation modeling in order to estimate the sound pressure at the desired points of the control areas. In the specific case of outdoor sound propagation models we can distinguish between geometrical acoustics based methods, diffuse field methods and wave-based methods [3]. In any case, the uncertainties in the parameters of the model such as sources' responses, weather conditions or acoustic properties of the materials in the propagation path can lead into poor predictions of the transfer functions. Robust optimization applied to sound field control has shown promising results introducing regularization terms directly proportional to the uncertainties in the parameters of the model [4]. Finding and reducing these uncertainties is important in order to get optimized solutions that are not over regularized, which will mean an over robust solution and poor performance of the acoustic control strategy.

Bayesian inference provides a framework to study uncertainties of a model based on data [5]. The hypothesis of this paper is that Bayesian inference is a suitable framework to quantify and reduce the uncertainty of acoustic parameters in models when data is available. This framework has been shown to work in similar regression problems in relevant engineering fields. Jeong et al. used it to characterize the flow resistivity of a sound absorber from reverberation chamber measurements [6]. Sadri et al. successfully improved the performance of a Statistical Energy model of a railway coach [7].

In this work a first insight on modeling acoustic sources from real data measurements applying the method presented in [1] is shown. The directivity response of a loudspeaker is measured in anechoic conditions and the amplitude and phase of a monopole model with directional amplitude is fitted to the measurements. The paper explains step by step how Bayesian inference can be used in such a case and sets the foundation to new research using the acoustic

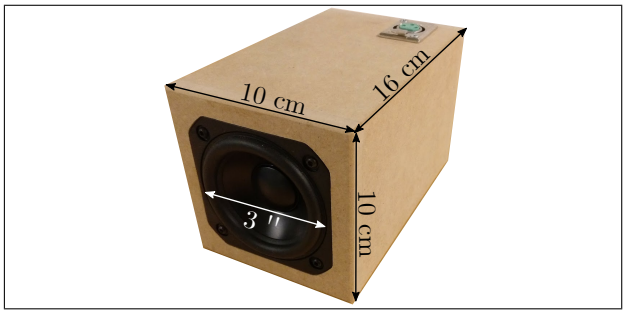

Figure 1. Loudspeaker unit used during the measurements.

source model developed in future sound field control experiments. The paper is structured as follows. Section 2 presents the methods and is structured in two main subsections. Section 2.1 describes first the setup and measurements of the directivity response, then the monopole model with complex amplitude used as generative model of the Bayesian inference and finally the statistical model used during the inference. Section 2.2 summarizes the Hamiltonian Monte Carlo sampling method used to find the posterior distribution. In Section 3 the methods are applied to directional impulse responses measured in free field conditions and results are shown and Section 4 presents the analysis of the results. Section 5 discuss the applied methodology and presents future challenges and Section 6 summarizes the present work.

2. Methods

In this section the directivity measurements and the monopole model are presented, and the estimation of the parameters of the model via Bayesian inference is explained. Finally Hamiltonian Monte Carlo sampling is summarized.

2.1. Bayesian Inference and Parameter Estimation

Bayesian inference is the process of fitting a probability model to a set of data and summarizing the result by a probability distribution on the parameters of the model [5]. This probabilistic model is updated as more evidence or information is available. In this section data, acoustic source model and statistical model are presented.

2.1.1. Data

Accurate measurements of the directivity of 3 different units of the same loudspeaker model were measured in free-field conditions. The directivity is only measured on the azimuth angle. Figure 1 shows one of the units and Figure 2 details the setup of the measurements.

The loudspeaker is mounted on a turntable and three microphones are placed in front of the source at the defined distances. The loudspeaker is rotated from

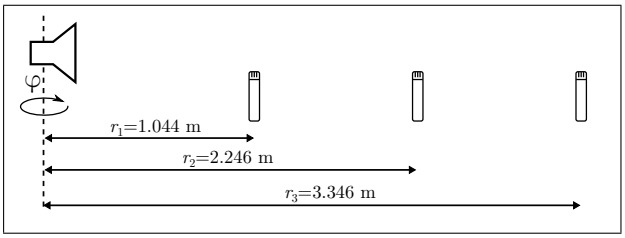

Figure 2. Schematic of the measurement setup.

$\varphi = 0$ to 360° playing a sine sweep every 5° (number of angles measured N_d= 72). Frequencies from 500 to 1000 Hz with a frequency resolution of Δf = 100 Hz are used in this work (number of frequencies measured N_f= 6).

2.1.2. Acoustic Source Model

The sound pressure created by a monopole at any position r can be written as

$$p = \frac{A \exp(\mathrm{j}(\omega t - kr))}{r}, \tag{1}$$

where k is the wavenumber, r is the distance to the monopole and A is a complex amplitude.

In real sound field control scenarios loudspeakers are used. Fitting A and r in Eq. (1) to a loudspeaker response is equivalent to finding the so called *acoustic center*, defined as "the point from which the approximately spherical wavefronts appear to diverge" [8]. In addition, loudspeakers will usually have directional response, presenting radiation patterns at different frequencies which are dependent on the geometry and size of the source. This means that both A and r need to be function of frequency and angle ($A(f, \varphi)$ and $r(f, \varphi)$).

2.1.3. Bayes' theorem and data fitting

The basis of Bayesian inference is the well known Bayes' theorem. Given N noisy sound pressure measurements $\tilde{\mathbf{p}}_{i,j} = \mathbf{p}_{i,j} + \mathbf{n}_{i,j}$ at $i = 1...N_f$ frequencies and $j = 1...N_d$ angles, the Bayes theorem can be written as

$$\pi(\theta|\tilde{\mathbf{p}}_{i,j}, M) = \frac{\pi(\tilde{\mathbf{p}}_{i,j}|\theta, M)\pi(\theta|M)}{\pi(\tilde{\mathbf{p}}_{i,j}|M)}, \tag{2}$$

where π is the probability density function and θ are the parameters included in the model M. Every function involved in (2) has a particular and well known name

$$posterior = \frac{likelihood \times prior}{evidence}.$$

Given a particular model, the aim of Bayesian inference is to find the *posterior* distribution, which

means to find the distribution for every parameter conditioned to the data. One of the advantages of the Bayesian framework is that prior knowledge about the experiment and the different parameters can be easily included in the formulation via the prior distribution, influencing the posterior distribution.

The posterior distribution is proportional to the *likelihood* and the *prior* distributions. Because the *evidence* is common for all the parameters given a particular model, it is usual to see Eq. (2) written as

$$\pi(\theta|\tilde{\mathbf{p}}_{i,j}, M) \propto \pi(\tilde{\mathbf{p}}_{i,j}|\theta, M)\pi(\theta|M). \tag{3}$$

If the noise is normally distributed $\mathbf{n} \sim \mathcal{N}(0, \sigma_{i,j})$, the likelihood distribution will be normally distributed

$$\pi(\tilde{\mathbf{p}}_{i,j}|\theta) = \prod_{n=1}^{N} \frac{\exp\left(-\frac{1}{2\sigma_{i,j}^2}\left(\tilde{p}_{i,j}^n - p_{i,j}^M(\theta)\right)^2\right)}{\sqrt{2\pi\sigma_{i,j}}}, \tag{4}$$

where $p^M(\theta)$ stands for the estimated pressure using model M.

2.1.4. Bayesian inference model of the acoustic source

In this section the Bayesian model is presented and the dependency between the different parameters of the problem explained.
Eq. (1) is used as the mean of the generative process of the data in Eq. (4), including a correction factor in the acoustic dispersion as follows (time domain dependency is dropped)

$$p_{i,j}^M = \frac{A_{i,j}\exp(-\mathrm{j}k_i r)}{r + \Delta r_{i,j}}. \tag{5}$$

The correction $\Delta r_{i,j}$ is introduced in order to model the steepness of the dispersion accounting for the effect of the apparent acoustic center position. This correction is not explicitly included in the phase, but implicitly in the complex amplitude A. Another difference with Eq. (1) is that $A_{i,j}$ is now dependent on frequency and azimuth angle, accounting for the directivity of the source. Because Bayesian inference applied to complex numbers is still to be developed in the used software environment, the problem is split into real and imaginary parts for each frequency and direction as follows

$$\Re(p_{i,j}^M) = \frac{A_{real}\cos(kr) + A_{imag}\sin(kr)}{r + \Delta r}, \tag{6}$$

$$\Im(p_{i,j}^M) = \frac{A_{imag}\cos(kr) - A_{real}\sin(kr)}{r + \Delta r}. \tag{7}$$

Two different models, named Model A and Model B respectively, are investigated. Figures 3 and 4 show

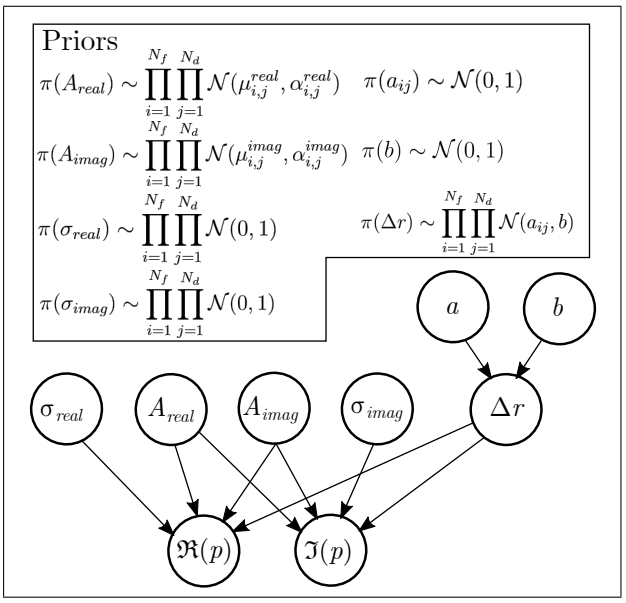

Figure 3. Inference diagram describing the relationship between the parameters and their prior distributions in Model A.

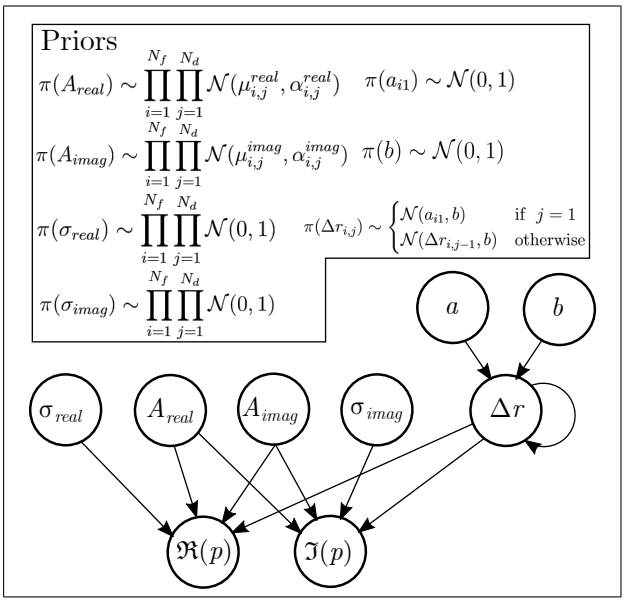

Figure 4. Inference diagram describing the relationship between the parameters and their prior distirbutions in Model B.

the relationship between the parameters of the models as well as the prior distributions.

All the parameters are considered normally distributed. The support of the parameters modeling variances, b and σ_x, is $(0, \infty)$. The standard deviation of the noise process $\sigma_{i,j}$ is also split in σ_{real} and σ_{imag}. The parameters $\mu_{i,j}^x$ and $\alpha_{i,j}^x$ of the prior distributions of the real and imaginary parts of A are computed from measurements using Eq. (1). The dispersion correction Δr is modeled in a hierarchical way by two hyperparameters a and b which are the mean and variance respectively. The only difference between

both models is the assumption of angular smoothness in Model B. To do so, Δr is modeled with a Kalman filter [9], which conditions the prior of $\Delta r_{i,j}$ to have the mean in the previous angle $\Delta r_{i,j-1}$. It implies that during the sampling procedure explained in the following section, the next sample from $\Delta r_{i,j}$ comes from a normal distribution with mean the current sample of $\Delta r_{i,j-1}$.

2.2. Sampling

Finding a closed solution to Eq. (2) is most likely intractable. A common approach to approximate the posterior distribution are the sampling methods. These methods are based on obtaining random samples θ^s from the desired distribution $p(\theta|\tilde{\mathbf{p}})$. There exist many different sampling techniques such as rejection sampling, importance sampling and Markov chain simulations to mention a few [5]. In this work a specific sampling method called No-U-Turn Sampler Hamiltonian Monte Carlo (NUTS HMC) is used. A small summary of the method is written in this section. For detailed explanation please follow Chapter 5 from [10] for HMC and [11] for NUTS.

HMC is based on the Hamilton's equations taking advantage of physics' intuition and removing the local random walk behavior of other sampling methods. Samples are drawn from a joint distribution $\pi(\theta, \phi)$ where ϕ is an auxiliary momentum variable with the same dimensions as θ. Usually ϕ is a multivariate normal that does not depend on θ

$$\phi \sim \mathcal{N}(0, \Sigma_\phi). \tag{8}$$

The joint density defines what is called the Hamiltonian

$$H(\phi,\theta) = -\log\pi(\phi,\theta) = -\log\pi(\phi|\theta) - \log\pi(\theta) = \tag{9}$$

$$= \underbrace{T(\phi|\theta)}_{kinetic\ energy} + \underbrace{V(\theta)}_{potential\ energy}.$$

To generate a transition between states of the joint distribution $\pi(\theta, \phi)$, one should consider Hamilton's equations and differentiate with respect to time

$$\frac{\mathrm{d}\theta}{\mathrm{d}t} = +\frac{\partial H}{\partial \phi} = +\frac{\partial T}{\partial \phi} \tag{10}$$

$$,\frac{\mathrm{d}\phi}{\mathrm{d}t} = -\frac{\partial H}{\partial \theta} = -\frac{\partial T}{\partial \theta} - \frac{\partial V}{\partial \theta} = -\frac{\partial V}{\partial \theta}. \tag{11}$$

Because the probability density function of ϕ is independent of θ, the first term of Eq.(11) is zero. According to this, a two-state differential equation has to be solved to update the state of the joint distribution. Most HMC implementations use the leapfrog integrator, which can be summarized in three steps (Chapter 12 from [5]).

1. Pick a random sample from the momentum variable $\phi \sim \mathcal{N}(0, \Sigma_\phi)$.
2. Take L leapfrog steps as follows.
   (a) $\phi \leftarrow \phi - \frac{1}{2}\varepsilon\frac{\mathrm{d}V}{\mathrm{d}\theta}$,
   (b) $\theta \leftarrow \theta + \varepsilon\Sigma_\phi\phi$,
   (c) $\phi \leftarrow \phi - \frac{1}{2}\varepsilon\frac{\mathrm{d}V}{\mathrm{d}\theta}$,
   where ε is a scaling factor and $\frac{\mathrm{d}V}{\mathrm{d}\theta} = -\frac{\mathrm{d}\log\pi(\theta|\tilde{\mathbf{p}})}{\mathrm{d}\theta}$. Because the Hamiltonian has energy conservation, getting closer to lower probability regions increases the potential energy and reduces the kinetic energy and vice versa, allowing easy exploration of high probability regions.
3. The new candidate sample θ^*, ϕ^* is the one drawn after L steps. This new sample is accepted with the following condition

$$\theta^t = \begin{cases} \theta^* & \text{with probability } \min(r, 1), \\ \theta^{t-1} & \text{otherwise,} \end{cases} \tag{12}$$

where $r = \frac{\pi(\theta^*|\tilde{\mathbf{p}})\pi(\phi^*)}{\pi(\theta^{t-1}|\tilde{\mathbf{p}})\pi(\phi^{t-1})}$.

One of the challenging points of using HMC is to tune the parameters ε and L. Hoffman et al. [11] proposed an adaptive procedure called No-U-Turn Sampler (NUTS) which tunes automatically the aforementioned parameters. This routine together with HMC is tedious to implement so the existing platform for statistical modelling Stan [12] is used, which provides an intuitive framework and computes NUTS HMC when running the inferences.

2.2.1. Assessing Convergence

When running sampling methods it is necessary to define a criteria to asses convergence. A useful method is to run several sequences starting from different dispersed points in the parameter space and monitor the convergence between and within sequences until stationarity is achieved [5]. In other words, when the distribution of a single sequence is similar to the mixed distribution of all the sequences, sampling is getting close to convergence. With a set of samples ψ_{lq} where $l = 1, ..., L$ is the length of each sequence and $q = 1, ..., Q$ is the number of sequences, the between- and within-sequence variances are

$$B = \frac{L}{Q-1}\sum_{q=1}^{Q}(\overline{\psi}_{.q} - \overline{\psi}_{..}), \tag{13}$$

$$\text{where } \overline{\psi}_{.q} = \frac{1}{L}\sum_{l=1}^{L}\psi_{lq},\ \overline{\psi}_{..} = \frac{1}{Q}\sum_{q=1}^{Q}\overline{\psi}_{.q},$$

and

$$W = \frac{1}{Q}\sum_{q=1}^{Q}s_q^2, \tag{14}$$

$$\text{where } s_q^2 = \frac{1}{L-1}\sum_{l=1}^{L}(\psi_{lq} - \overline{\psi}_{.q})^2,$$

respectively. The convergence can be monitored by the factor $\hat{R}$ [5], an estimate of the scale by which the current distribution ψ might be reduced if $L \to \infty$

$$\hat{R} = \sqrt{\frac{\widehat{\text{var}}^{+}(\psi|\mathbf{p})}{W}}, \tag{15}$$

where

$$\widehat{\text{var}}^{+}(\psi|\tilde{\mathbf{p}}) = \frac{L-1}{L}W + \frac{1}{Q}B. \tag{16}$$

$\hat{R}$ tends to 1 when $L \to \infty$ and if it is high then there exist a chance to improve the inferences by running longer sequences.

3. Results

In this section the results of running NUTS HMC with Stan over the two mentioned models are presented. Four sampling sequences of 2000 samples are initialized at random initial values. The first half of the samples drawn are considered warm up samples and are discarded to compute inference summaries. The total amount of parameters fitted is 1333 in Model A ($N_d \times N_f \times 6+1$) and 1117 in Model B ($N_d \times N_f \times 5+7$). The mean and standard deviations of the prior distributions of A_{real} and A_{imag} are calculated as follows

$$\begin{aligned}
\mu_{i,j}^{real} &= \overline{r\left((\Re(\tilde{\mathbf{p}}_{i,j})\cos(k_i r) - \Im(\tilde{\mathbf{p}}_{i,j})\sin(k_i r)\right)}, \\
\mu_{i,j}^{imag} &= \overline{r(\Im(\tilde{\mathbf{p}}_{i,j})\cos(k_i r) + \Re(\tilde{\mathbf{p}}_{i,j})\sin(k_i r))}, \\
\alpha_{i,j}^{real} &= 4\ \text{Var}\left(r(\Re(\tilde{\mathbf{p}}_{i,j})\cos(k_i r) - \Im(\tilde{\mathbf{p}}_{i,j})\sin(k_i r))\right), \\
\alpha_{i,j}^{imag} &= 4\ \text{Var}\left(r(\Im(\tilde{\mathbf{p}}_{i,j})\cos(k_i r) + \Re(\tilde{\mathbf{p}}_{i,j})\sin(k_i r))\right).
\end{aligned}$$

The variance is chosen less informative (multiplied by a factor of 4) avoiding over constrains in the models and leading to a better analysis of their robustness when sampling from a wider space. Figures 5 and 6 show prior vs. posterior samples of the joint distributions (A_{real}, A_{imag}) and (a, b) respectively. Marginal prior and posterior distributions are also plotted with kernel density estimation on the frame of the figures.

Figure 7 shows the mean and standard deviation of the inferred parameter Δr for both models at three different frequencies 600, 800 and 1000 Hz. Model A is plotted in full line and Model B in dashed line. The same is shown for A_{real} and A_{imag} in Figures 8 and 9 respectively.

The factor $\hat{R}$ is plotted for all the parameters of both models in Figure 10. Because Model B only defines one a per frequency but doesn't distinguish per angle, for a given frequency i each $a_{i,j}$ from Model A is compared to a_i in Model B.

The log-likelihood is presented in Figure 11 for the data recorded at each microphone and the error between the data and the samples drawn is plotted in Figure 12 per frequency and angle.

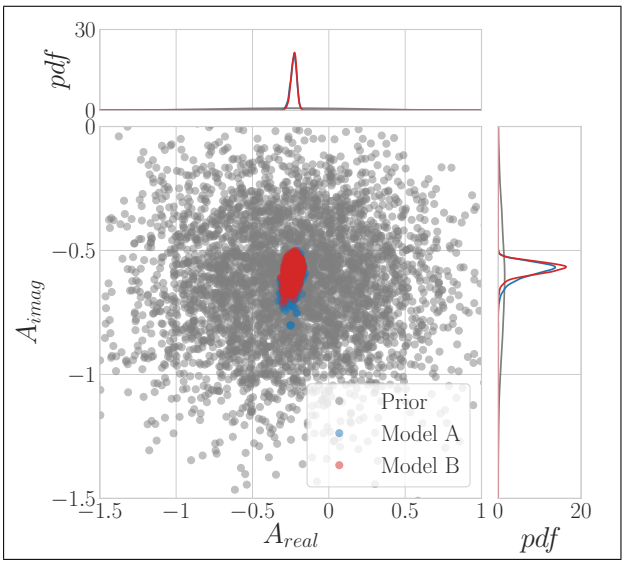

Figure 5. Prior vs. Posterior samples of the complex amplitude A. Frequency: 900 Hz. Angle: 150 °.

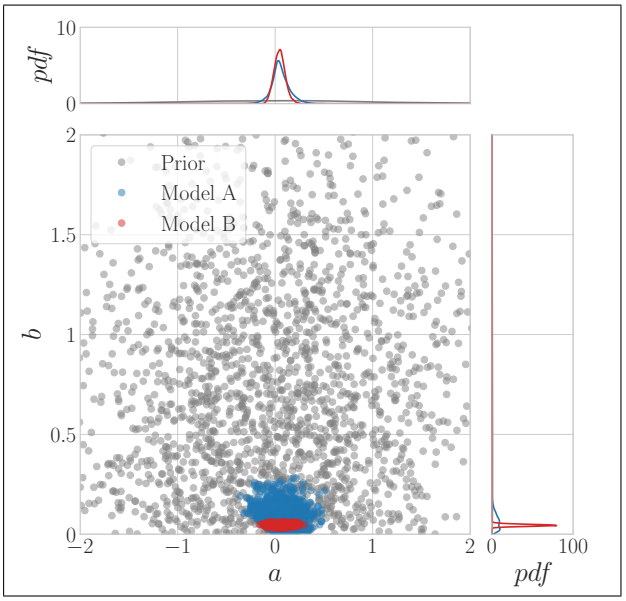

Figure 6. Prior vs. Posterior samples of the hyperparameters a and b. Frequency: 900 Hz. Angle: 150 °.

4. Analysis

In this section the analysis of the results shown in the previous section is presented.

From visual inspection of Figures 5 and 6 both models present a very sharp posterior distribution, showing Model B a narrower posterior on parameter b for the chosen frequency and angle. This can be seen also in Figures 7, 8 and 9 where the Kalman smoothing reduces the variance. The variation in standard deviation between models for all the parameters is presented in Figure 13. It shows the standard deviation difference in percentage between both models $\Delta STD = \frac{STD_B - STD_A}{STD_A} \times 100$.

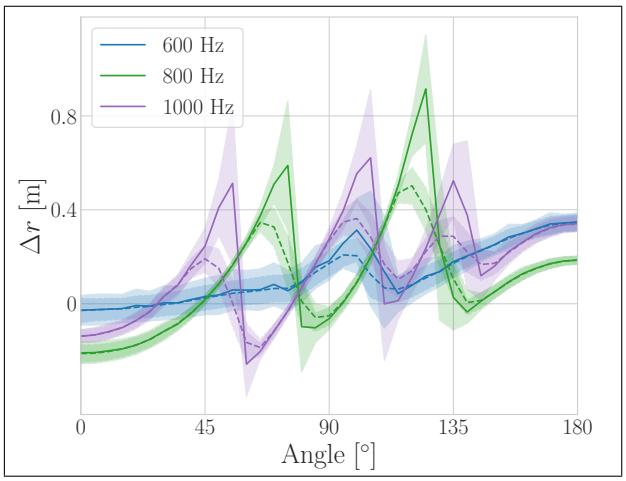

Figure 7. Dispersion correction Dr. −: Model A. −−: Model B. Mean and standard deviation of the posterior is plotted for three different frequencies, 600, 800 and 1000 Hz.

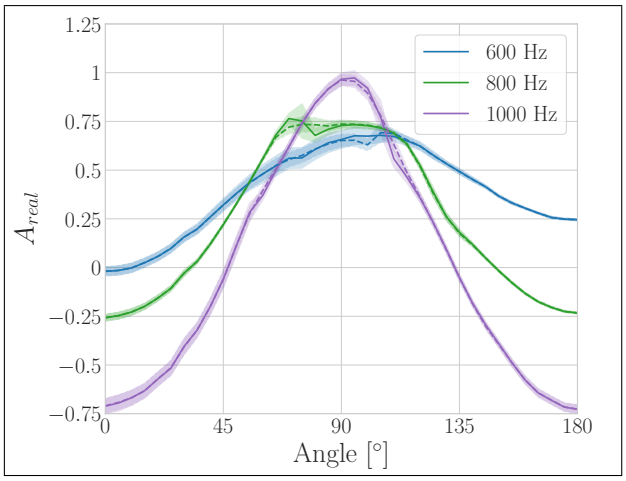

Figure 8. Real part of the directional amplitude A_{real}. −: Model A. −−: Model B. Mean and standard deviation of the posterior is plotted for three different frequencies, 600, 800 and 1000 Hz.

The uncertainty of most of the parameters is reduced by more than 50% when using Kalman filtering, except a few outliers where Model B fails to fit the data. These outliers are also seen in Figure 10 presenting a bad convergence for four parameters where $\hat{R} > 2$. All these parameters correspond always to $f = 600$ Hz and $\varphi = 105°$, which could mean an error in the measurements at that particular frequency and angle.

One way of checking which part of the parameter space is problematic is to study divergent transitions during HMC sampling [13]. If many divergent transitions occur it means that the inference has to be studied carefully as the parameter space wasn't explored properly. Model B has no divergences while Model A presents 6% of divergent transitions. Figure 14 shows all the sampling sequences for all the parameters distinguishing between divergent and non-divergent transitions. It can be seen a concentration of the divergences when b gets closer to 0.

The likelihood shows overfitting of the data recorded by the second microphone for both models.

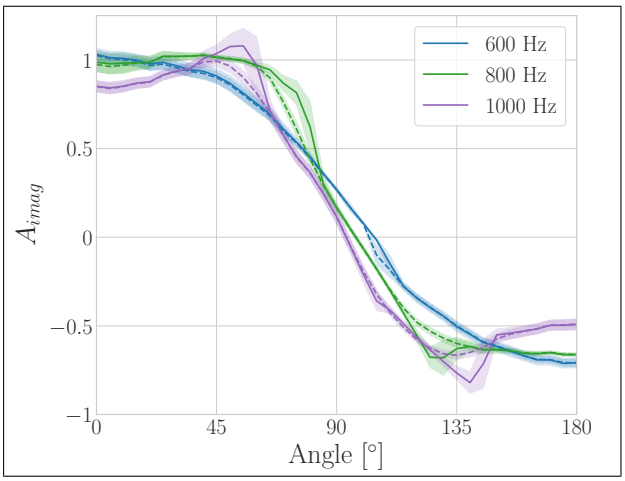

Figure 9. Imaginary part of the directional amplitude A_{imag}. −: Model A. −−: Model B. Mean and standard deviation of the posterior is plotted for three different frequencies, 600, 800 and 1000 Hz.

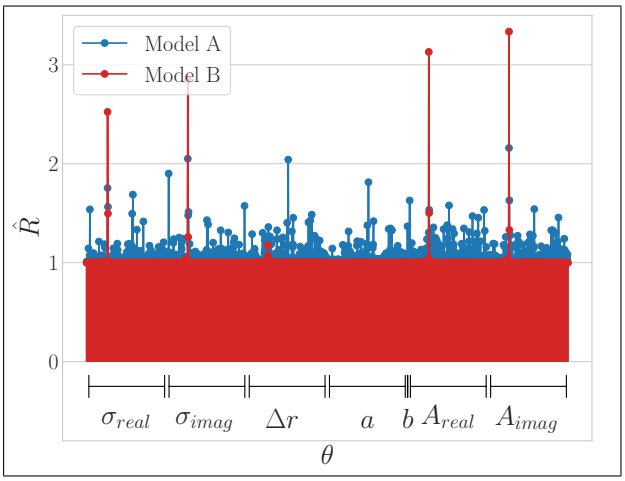

Figure 10. Scale parameter $\hat{R}$ for all the parameters of the problem.

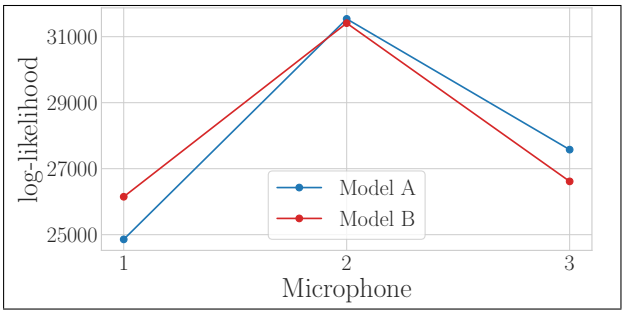

Figure 11. Total log-likelihood for the data recorded by each microphone.

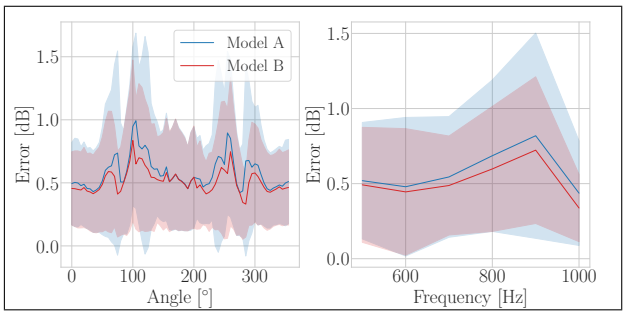

Figure 12. Error in dB between data and inferences. Left: Summary over all the frequencies. Right: Summary over all the angles.

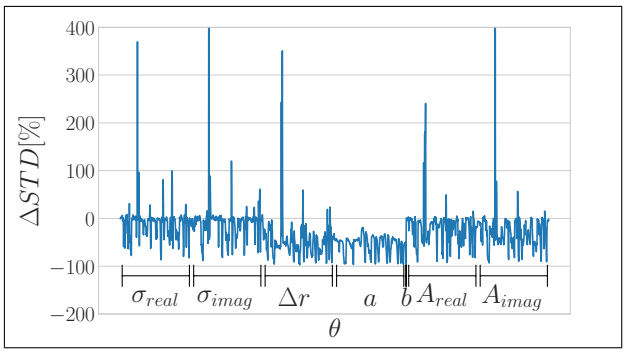

Figure 13. Difference in the standard deviation of both models.

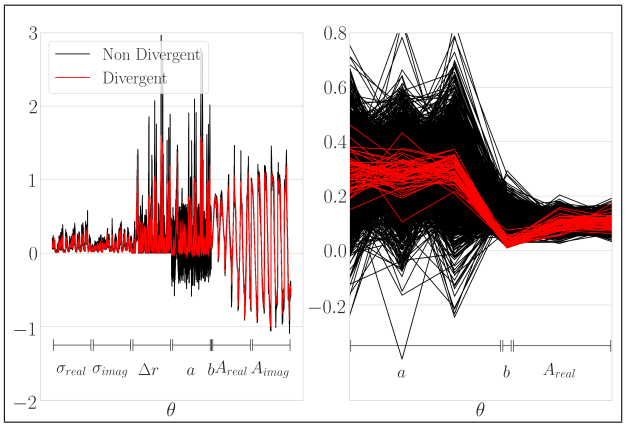

Figure 14. Divergent transitions during sampling Model A. The left plot shows all the transitions for all the parameters. The right plot zooms around parameter b.

Model B equalizes the fitting of microphones 1 and 3 while keeping the same performance for microphone 2. Looking at Figure 12, Model B shows less error in general, presenting higher improvement at higher frequencies and reducing significantly the uncertainty for all frequencies and angles.

5. Discussion

During this section the pros and cons of each model are discussed, especially those that are more relevant in outdoor sound field control schemes.

The introduction of Kalman filtering in Model B is equivalent to regularizing the solution, smoothing the transitions between angles not only in Δr but also in A, which would favor the reduction of artifacts. Moreover, Δr doesn't reach as high values as it does in Model A. However the problem is not as sensitive to changes in Δr as it is to changes in A, which is due to the fact that A models both amplitude and phase of the data, while Δr is only part of the amplitude. This difference in sensitivity can be seen in the low variance in the posterior distributions of A compared to the variance in Δr. The error between model and data is reduced when using Kalman filtering. However, it is still quite high, with a standard deviation above 1 dB in some cases, showing the difficulty of fitting a far field model to such measurements.

Both models overfit the data from microphone 2 compared to recorded pressure at microphones 1 and 3. This seems to arise from the experiment setup. The rotation point is not taken at the diaphragm but at 9 cm to the back of the loudspeaker. That means that the directivity pattern changes depending on the microphone considered unless the measurements are taken in the far field. This means that A and Δr, which are assumed to be independent of microphone position try to fit data that doesn't follow that assumption when close to the source.

Stability is another issue that has to be studied, specially if the sound field control strategy relies on the convergence of the inferences. Model B presented a consistent inference with execution time always below 3 minutes, showing the same behavior for any random initialization of the HMC. Model A strongly depends on the initialization samples, not always converging and varying from 10 to 30 minutes the execution time for several runs tried. According to Section 2.2.1 and Figure 10, longer sampling sequences would end in better inferences for Model A. However, the improvement wasn't significant when trying 4000 samples. One way of improving Model A stability is by getting rid of the divergences. Divergences occur where the curvature of the posterior is too high and the sampling routine fails to explore that region. In this case, parameter b provokes divergent transitions when sampling close to 0. Comparing to the posterior found by Model B it seems reasonable that HMC tries to explore that area. One way of solving this problem is by rescaling the prior distribution to a narrower one. A small hint to keep computational stability in Stan, is that it is usually better to sample from a generic distribution $\mathcal{N}(0,1)$ and then multiply each sample by a scaling factor $\beta << 1$ than sampling directly from $\mathcal{N}(0,\beta)$. Another way of trying to get around of divergences is

by reducing the step size of the HMC routine.

One main drawback of this simplified model is the lack of parameterization in its formulation. If it is used as a source model in another scenario where the angles to be assessed are different from the ones used in this optimization, interpolation is necessary. It seems reasonable that Model B would behave better than Model A in that regard due to its smooth shape, but this is something that should be tested.

As future research, spherical harmonics could be a good model because they include angular parameterization by the Legendre functions. Another option is to refit the presented models in every new scenario for the desired angles and frequencies, using the loudspeakers' manufacturers frequency responses as the mean of the normal processes of A and fitting the model when playing several units at the same time, as it happens in sound field control scenarios. If the frequency resolution is high enough it is worth trying to link both angles and frequencies through smooth transitions via Kalman filtering, so the posterior is conditioned to more data at the same time.

6. Conclusions

In sound field control, the precise knowledge of transfer functions in the control areas is crucial. A Bayesian approach was proposed to update acoustic models that can be used for estimating the transfer functions instead of direct measurements. As a case of study the directivity response of three different units of the same loudspeaker model were measured and modeled using a monopole model and Bayesian framework. It was shown that Bayesian inference is a proper framework for dealing with inverse problems with uncertainties, increasing the accuracy of the predictions when used wisely. Prior knowledge has a big impact in the inferences. Smooth angular transitions in the directivity response is incorporated by tweaking the prior distributions using a Kalman filter between angles. The influence of the filter is evident in the results presenting much smoother solutions. The error was also reduced and the model was in general more stable. Overfitting was slightly reduced but the error of fitting a far field model to directivity response data is still present, showing the need of a more suitable model for this problem. It was also shown how convergence has to be studied when running sampling methods for approximating the posterior distributions. It helps to understand where are the weak points of the models and to know if the inferences can be trusted or not.

Acknowledgement

I would like to thank Franz Heuchel for working together all day long in this project. Henrik Hvidberg, Jørgen Rasmussen and Tom A. Petersen for helping setting up all the experiments. And Jonas Brunskog, Efrén Fernández Grande and Finn T. Agerkvist for all the valuable discussions.

This project has received funding from the European Union's Horizon 2020 research and innovation programme under grant agreement No 732350.

References

[1] F. M. Heuchel, D. Caviedes Nozal, J. Brunskog, E. Fernandez Grande, and F. T. Agerkvist, "An adaptive, data driven sound field control strategy for outdoor concerts," 2017.

[2] M. Olsen and M. B. Møller, "Sound zones: on the effect of ambient temperature variations in feedforward systems," in *AES 142nd Convention*, 2017.

[3] M. Hornikx, "Ten questions concerning computational urban acoustics," *Building and Environment*, 2016.

[4] Q. Zhu, P. Coleman, M. Wu, and J. Yang, "Robust Acoustic Contrast Control with Reduced In-situ Measurement by Acoustic Modeling," *Journal of the Audio Engineering Society*, vol. 65, pp. 460–473, jun 2017.

[5] A. Gelman, J. B. Carlin, H. S. Stern, D. B. Dunson, A. Vehtari, and D. B. Rubin, *Bayesian Data Analysis*. Boca Raton: Chapman and Hall, third ed., mar 2013.

[6] C.-h. Jeong, S.-H. Choi, and I. Lee, "Bayesian inference of the flow resistivity of a sound absorber and the room's influence on the Sabine absorption coefficientsa)," *The Journal of the Acoustical Society of America*, vol. 141, pp. 1711–1714, mar 2017.

[7] M. Sadri, J. Brunskog, and D. Younesian, "Application of a Bayesian algorithm for the Statistical Energy model updating of a railway coach," *Applied Acoustics*, vol. 112, pp. 84–107, 2016.

[8] S. Barrera-Figueroa, K. Rasmussen, and F. Jacobsen, "The acoustic center of laboratory standard microphones," *Journal of the Acoustical Society of America*, vol. 120, no. November 2006, pp. 2668–2675, 2006.

[9] A. Aravkin, J. V. Burke, L. Ljung, A. Lozano, and G. Pillonetto, "Generalized Kalman Smoothing: Modeling and Algorithms," 2016.

[10] S. Brooks, A. Gelman, G. L. Jones, and X.-L. Meng, eds., *Handbook of Markov Chain Monte Carlo*. Chapman & Hall/CRC, first ed., 2011.

[11] M. D. Hoffman and A. Gelman, "The No-U-Turn Sampler: Adaptively Setting Path Lengths in Hamiltonian Monte Carlo," nov 2011.

[12] "Stan probabilistic programming language.." `http://mc-stan.org/`. Accessed: 26-03-2018.

[13] M. J. Betancourt and M. Girolami, "Hamiltonian Monte Carlo for Hierarchical Models," dec 2013.